applied sciences

MDPI

Article

Stability Analysis of High and Steep Slopes Considering Fault in Abandoned Mine Pit-Converted Pumped-Storage Power Station Reservoir During Pre-Impoundment Stage

Huihui Jia [1,2,3], Qiaoling Min [1,*], Mengxi Zhang [1,4], Shuai Han [5], Jingyi Zhang [1] and Chen Xu [1,6]

[1] State Key Laboratory of Hydraulic Engineering Intelligent Construction and Operation, Tianjin University, Tianjin 300350, China; magic-jia@163.com (H.J.)
[2] Geological Disaster Monitoring and Early Warning Technology Innovation Center of Hebei Province, Chengde 067000, China
[3] He Bei Hua Kan Resource Environmental Survey Co., Ltd., Chengde 067000, China
[4] School of Water Resources and Hydropower Engineering, Xinjiang Polytechnic Institute, Hotan 848023, China
[5] Department of Building and Real Estate, Hong Kong Polytechnic University, Hong Kong 999077, China
[6] School of Resource and Environment Engineering, Wuhan University of Technology, Wuhan 430070, China
* Correspondence: mql2012@tju.edu.cn

Abstract

The transformation of abandoned open-pit mines into pumped-storage power station reservoirs offers an effective way to optimize China's energy structure and supports China's dual-carbon objectives by providing large-scale flexible storage. However, the steep slopes and complex geological conditions formed by mine excavation pose severe challenges to the stability of reservoir slopes. This paper focuses on a pumped-storage power station project converted from an abandoned mine pit in Luanping, Hebei Province. Specifically addressing high and steep slopes containing weak faults, it proposes a stability analysis method for the excavation stage that considers the influence of faults. The analysis assumes dry conditions, excluding reservoir-induced pore water pressure and seepage forces. Adopting the Janbu method and the M-P method within the limit equilibrium framework, safety analyses were conducted on multiple typical analysis sections of the abandoned mine pit before and after excavation. Analytical results indicate that the minimum safety factors derived from the Janbu method pre- and post-excavation are 1.33 and 2.13, respectively, whereas those obtained via the M-P method are 1.40 and 2.47. Given its consistently lower and thus more rigorous estimations, the Janbu method is recommended for conservative engineering design and risk assessment in similar geological settings. It is found that when the fault outcrop daylighting on the slope face constitutes a substantial spatial proportion, the potential sliding surface of the slope will extend from the top of the weak fault along an arc to the bottom of the stepped excavation. This indicates that the position of the fault influences both the sliding mode and the safety performance of the slope. The research findings of this paper could provide technical support for the slope engineering design, excavation and construction of pumped-storage power station reservoirs converted from abandoned mine pits.

Keywords: abandoned mine pit; pumped-storage power station; fault; limit equilibrium method; slope stability

Check for updates

Academic Editor: Roohollah Kalatehjari

Received: 5 July 2026
Revised: 27 August 2026
Accepted: 1 September 2026
Published: 9 September 2026

1. Introduction

With the introduction of China's Dual Carbon Goals (Carbon Peaking and Carbon Neutrality), the share of renewable energy in the nation's energy mix is continually growing. However, the inherent intermittency and volatility of renewable sources, particularly solar and wind power, present a severe challenge to stable power grid operation. Consequently, the importance of large-scale energy storage technologies is becoming increasingly prominent. Among these, Pumped Storage Hydropower (PSH) stations have emerged as the most widely implemented and most economically viable method for large-scale power system energy storage, leveraging their core advantages: technical maturity, operational reliability, large capacity, and long lifespan. In recent years, the repurposing of abandoned open-pit mines as pumped storage power station reservoirs has emerged as a key research focus both domestically and internationally. Abandoned mine pits offer natural benefits for constructing both upper and lower reservoirs, primarily due to their unique deeply recessed topography and substantial spatial volume. This conversion strategy provides a multifaceted advantage: it enables significant conservation of land resources, preventing the acquisition of valuable farmland and forestland typically required for new reservoir sites, and it substantially minimizes the required volume of earthwork excavation and backfilling, consequently reducing overall project construction costs [1–4].

Despite the multifaceted advantages of this repurposing strategy, the complex geological environment inherent to abandoned open-pit mines introduces substantial geotechnical and engineering challenges. During long-term mining operations, open-pit mines typically form high, steep slopes. The geological structure of these slopes is often damaged to varying degrees, characterized by the development of joints, fissures, and even weak faults. Probabilistic modeling methods are frequently employed to study the distribution patterns of such geological bodies [5–7]. However, these unfavorable geological factors make the stability of reservoir slopes a critical issue affecting the safe operation of power stations. Qiao et al. [8] conducted a multi-field coupling analysis of seepage-stress-deformation after the excavation of an underground reservoir, finding that the rock mass deformation around the chamber of a typical pumped storage power station cross-section was low, and the safety met the requirements. Kafle et al. [9] used a numerical simulation method to deeply investigate the influence of rapid water level drawdown on the pore water pressure distribution and effective stress of high and steep rock slopes, revealing the progressive failure mechanism of slopes under hydro-mechanical coupling. Hu et al. [10] combined the CFD-DEM fluid-solid coupling method to analyze the influence of rock content and rock shape on slope stability under seepage action, finding that low rock content easily induces slope sliding issues. Of particular concern is the significant impact of faults on structures [11]. Weak faults, acting as potential sliding surfaces within slopes, play a crucial role in influencing slope stability and safety. Wang et al. [12] utilized a novel particle finite element method (PFEM) to study the instability and failure mechanism of rock slopes considering the effect of faults, realistically reproducing the temporal sequence of the slope failure process. Zeng et al. [13] employed machine learning methods to study the correlation between deep and surface deformation of excavated slopes under rainfall conditions and verified the accuracy using a typical excavated slope engineering case located along the edge of a strike-slip fault basin. Of particular note, the strength of soft interlayers, such as fault gouge and cataclasite, significantly decreases under saturated water conditions [14,15]. Consequently, evaluating the stability of high and steep slopes containing weak faults under dry construction-stage conditions is an essential step in controlling excavation-induced instability before reservoir impoundment. Commonly employed methods for slope stability analysis include the Strength Reduction Method [16–19], the Limit Equilibrium Method [20–24], and the Reliability Analysis Method [25–27]. The Limit Equilibrium Method is the most widely adopted technique in engineering practice, primarily

https://doi.org/10.3390/app16188953

owing to its computational simplicity and clear theoretical framework. This method provides an effective analytical tool for the safety assessment of high and steep slopes by calculating the safety factor. This calculation is achieved by assuming the soil or rock mass on the sliding surface is in a state of limit equilibrium and applying the fundamental conditions of force or moment equilibrium. Repurposing abandoned open-pit mines as pumped storage reservoirs requires further excavation of existing slopes, which inherently introduces the risk of sliding during construction. The presence of weak faults further exacerbates this risk. Consequently, it is imperative to adopt efficient methodologies to evaluate slope stability throughout the construction phase.

In summary, utilizing abandoned open-pit mines to convert them into pumped storage power station reservoirs is a highly promising sustainable development model. However, the presence of soft faults imposes higher requirements for the stability analysis of high and steep slopes. This paper is based on the project of a pumped storage power station reservoir converted from an abandoned mine in Luanping, Hebei Province. It proposes a stability analysis method for high and steep slopes, both before and after excavation, that considers the effect of faults. By identifying potential slope slip surfaces, the study investigates the influence of soft faults on slope safety. The findings are intended to support excavation design, construction sequencing, and slope-reinforcement decisions for abandoned open-pit mines converted into pumped-storage reservoirs before impoundment.

2. Theory and Methods for Slope Stability Analysis

According to the Technical Code for Non-Coal Open-Pit Mine Slope Engineering (GB 51016-2014) [28], slope stability calculations shall primarily adopt the Limit Equilibrium Method (LEM), with the safety factor (F_s) serving as the main evaluation index. For slopes in fractured rock masses and granular media, the Simplified Morgenstern-Price (M-P) method is recommended for stability calculations when the failure mode is circular or composite. For blocky rock slopes and layered rock slopes, the Janbu Method is recommended for stability calculations when the failure mode is composite or polyline (non-circular). Based on the specific geological and engineering characteristics of the project site, the Janbu Method and the Morgenstern-Price (M-P) Method were selected to conduct separate Limit Equilibrium Safety factor (F_s) analyses for the slope.

2.1. Janbu Limit Equilibrium Method

The Janbu method extends the original circular arc method to the case of an arbitrary slip surface. It assumes that the safety factor remains constant along the entire non-circular slip surface. The Janbu simplified method satisfies force equilibrium for each slice but does not strictly satisfy overall moment equilibrium. The calculation diagram is shown in Figure 1. Under this method, the slip surface during slope failure can be of any shape.

$$F_s = \frac{\sum [c_i l_i + (\Delta W_i + \Delta H_i)\tan\varphi_i]\frac{1}{m_{\theta_i}}}{\sum (\Delta W_i + \Delta H_i)\sin\theta_i} \quad (1)$$

where $m_{\theta i} = \cos\theta_i + \frac{\sin\theta_i \tan\varphi_i}{F_s}$. ΔW_i is the weight of the i-th slice (kN). c_i is the effective cohesion of the base of the i-th slice (kPa). φ_i is the internal friction angle of the base of the i-th slice (°). l_i represents the length of the i-th slice base (m). ΔH_i is the additional stress on the i-th slice (kN/m), and θ_i is the inclination angle of the slip surface of the i-th slice (°). R represents the radius of the circular slip surface (m) and F_s represents the safety factor against the slice sliding.

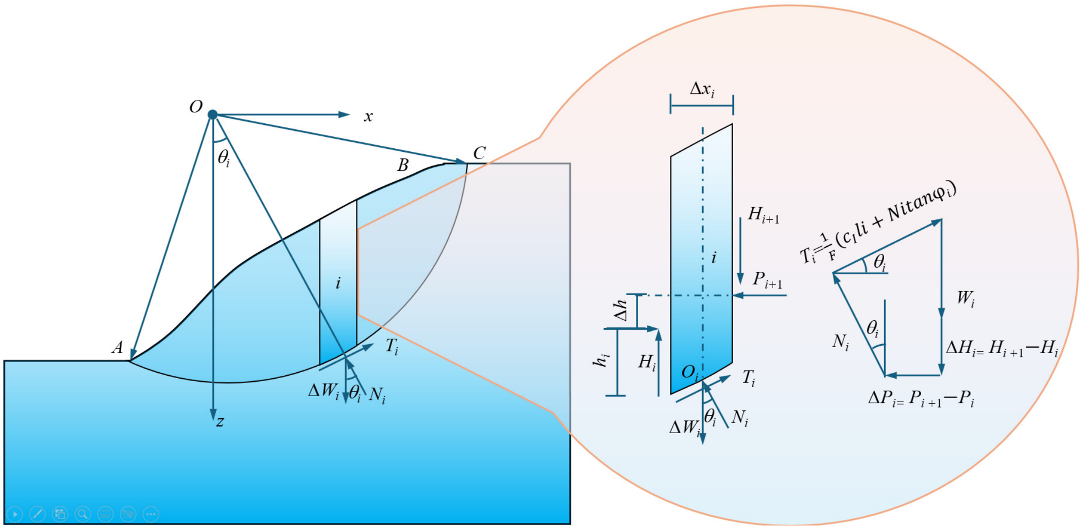

Figure 1. Calculation Diagram for the Janbu Method.

2.2. M-P Limit Equilibrium Method

The Morgenstern-Price (M-P) method is applicable to slip surfaces of arbitrary configuration. It satisfies the full conditions of static equilibrium by requiring that the vector sum of forces and the sum of moments for every individual soil slice are both equal to zero; the computational scheme is depicted in Figure 2. During the computation of the safety factor, the ratio of the shear inter-slice force X to the normal inter-slice force E for each slice is postulated as a function of the horizontal coordinate x. The minimum safety factor and the corresponding critical slip surface are subsequently determined by enforcing the boundary conditions applicable to the entire sliding soil mass.

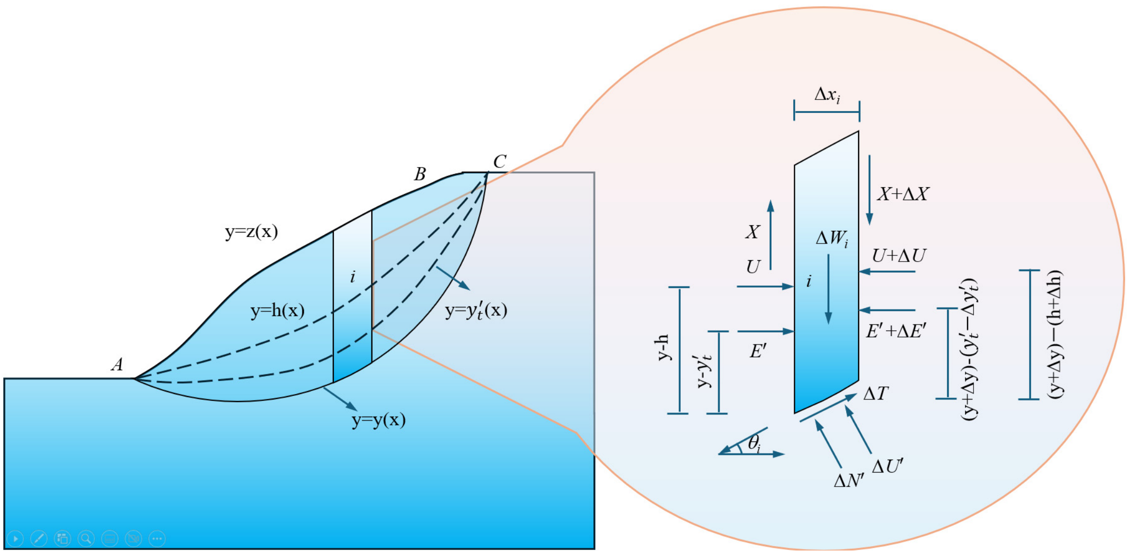

Figure 2. Computational Scheme for the M-P Method.

As illustrated in Figure 2, an arbitrarily shaped slope is represented, where the slope face, the thrust lines of the lateral pore water stress and effective stress, and the slip surface are denoted by the functions $y = z(x)$, $y = h(x)$, $y = y_t'(x)$ and $y = y(x)$ respectively. An arbitrary differential soil slice, Δx_i, within the slope is subjected to the force of gravity ΔW_i; the effective normal reaction force $\Delta N'$ and the tangential resistance ΔT acting on the base of the soil slice; the effective normal inter-slice forces E', $E' + \Delta E'$ and the inter-slice shear forces X, $X + \Delta X$ acting on the two sides of the soil slice. U and $U + \Delta U$ represent the pore

https://doi.org/10.3390/app16188953

water stresses acting on the sides of the slice, while $\Delta U'$ is the pore water stress acting on the base of the slice.

Based on the force system acting on the soil slice, the differential equation for force equilibrium of each slice is given by:

$$\begin{aligned}\frac{\Delta E\prime}{\Delta x}\left[1-\frac{tan\varphi}{F_s}\frac{\Delta y}{\Delta x}\right]+\frac{\Delta X}{\Delta x}\left[\frac{tan\varphi}{F_s}+\frac{\Delta y}{\Delta x}\right]\\ =\frac{c'}{F_s}\left[1+(\frac{\Delta y}{\Delta x})^2\right]+\frac{\Delta U}{\Delta x}\left[\frac{tan\varphi}{F_s}\frac{\Delta y}{\Delta x}-1\right]\\ +\frac{\Delta W}{\Delta x}\left\{\frac{tan\varphi}{F_s}+\frac{\Delta y}{\Delta x}-r_u\left[1+(\frac{\Delta y}{\Delta x})^2\right]\frac{tan\varphi}{F_s}\right\}\end{aligned} \quad (2)$$

For each soil slice, since the horizontal width Δx is infinitesimally small, the boundaries defined by $y = z(x)$, $y = h(x)$ and $y = y(x)$ can be approximated as linear within the extent of the slice. Similarly, the function $f(x)$ can also be assumed to be linear within the extent of each slice. Therefore, within each soil slice, the following relationship holds:

$$\begin{cases} y = Ax + B \\ \frac{\Delta W}{\Delta x} = px + q \\ f = kx + m \end{cases} \quad (3)$$

where A, B, p, q, k and m are arbitrary constants determined by the geometric conditions and the selected type of function.

Following the aforementioned derivations and approximations, the fundamental differential Equation (2) simplifies to:

$$(Kx+L)\frac{\Delta E}{\Delta x}+KE=Nx+P \quad (4)$$

The boundary conditions for the two sides of the soil slice are now taken as:

$$\begin{cases} E = E_i,(x = x_i) \\ E = E_{i+1},(x = x_{i+1}) \end{cases} \quad (5)$$

Integrating Equation (4) from x_i to x_{i+1} yields:

$$E_{i+1}=\frac{1}{L+K\Delta x}\left(E_iL+\frac{N\Delta x^2}{2}+P\Delta x\right) \quad (6)$$

This sequential process allows for the determination of the normal inter-slice force E from the top to the bottom of the slope, followed by the calculation of the inter-slice shear force X. When no other external forces act on the sliding soil mass, the following boundary condition must be satisfied for the last slice:

$$E_n = 0 \quad (7)$$

Simultaneously, the moment on the sides of the soil slice can be determined by integrating the differential Equation (8), which is expressed as:

$$M_{i+1}=E_{i+1}(y+y_t)_{i+1}=\int_{x_i}^{x_{i+1}}(X-E\frac{\Delta y}{\Delta x})\Delta x \quad (8)$$

Finally, the condition that must also be satisfied is:

$$M_n=\int_{x_0}^{x_n}X-E\frac{\Delta y}{\Delta x}\Delta x=0 \quad (9)$$

At this point, the location of the resultant inter-slice force application point, y_t, can be determined using Equation (8). To find the values of λ and F_s that satisfy all equilibrium equations, the calculation begins by assuming initial values for λ and F_s. This is followed by slice-by-slice integration to determine the resulting residual normal inter-slice force E_n and moment M_n. If these residuals are non-zero, λ and F_s are progressively adjusted through a systematic iterative process until both Equations (7) and (9) are satisfied. Consequently, the M-P method is fundamentally a cyclic iterative procedure.

2.3. Numerical Implementation Details

The slope stability analyses were performed using Slide2 6.0 (Rocscience Corporation, Toronto, ON, Canada), a widely recognized software for limit equilibrium slope stability analysis. To ensure the reproducibility and accuracy of the results, the following numerical parameters and methodologies were employed:

(a) Search algorithm for critical surfaces: Given the complex geological conditions involving weak faults, the critical slip surfaces are non-circular. A random search algorithm was then applied within the identified region to explore a large number of potential non-circular slip surfaces. This method is particularly effective for locating complex, fault-controlled slip surfaces that do not follow a simple geometric pattern.

(b) Discretization strategy: The sliding mass was discretized into vertical slices for the Janbu and M-P methods. To ensure computational precision while maintaining efficiency, the number of slices was set to 100 slices per meter of horizontal width. This discretization density ensures that the geometry of the slip surface, especially along the fault planes, is accurately represented.

(c) Convergence criteria: The iterative calculation for the safety factor was terminated when the difference between the safety factors of two consecutive iterations was less than 0.001. This strict convergence criterion ensures the reliability of the calculated minimum safety factors.

3. Introduction to the Engineering Case Study

3.1. Luanping Pumped Storage Power Station

The project area is located in the central section of the Yanshan Mountains in China. The terrain is characterized by a significant undulation, with elevations generally decreasing from the northwest to the southeast, forming a geomorphology that transitions from middle-to-low mountainous terrain to hilly topography. The project site is centered on Pingdingshan (Flat-Top Mountain), which represents the highest topographical point with a maximum elevation of 997 m. Three ridges extend outwards in a three-pronged configuration (trident-like), gradually descending toward the northeast, west, and south. To the east lies the relatively broad and gentle trough-valley topography of Shanghaqin Village, with elevations ranging from 540 m to 570 m, characterized by a northern high and southern low profile; to the west is the Yixun River Valley, which generally flows from the northeast to the southwest. The river course meanders through the project area, exhibiting a continuous "S"-shaped pattern, and forms a distinct "U"-shaped bend where it encounters the extending ridge on the western side. The riverbed elevation ranges from 460 m to 490 m; both banks of the river valley feature fluctuating peaks and are characterized by well-developed tributary gullies; to the south, at the foot of Pingdingshan, a relatively open and gentle gully is present. This feature generally exhibits a west-to-east decline in elevation, with altitudes ranging from 570 m to 600 m. The current topography and geomorphology of the project area are defined by an open-pit mine (or quarry). The mine pit generally exhibits an irregular configuration. Due to the historical bench mining operations, the interior of the pit comprises multi-level slopes (benches) and platforms, while the pit bottom remains flat. To promote the optimization and adjustment of China's energy structure and enhance the peak-shaving capacity of the Hebei provincial power grid, the abandoned mine pit has been planned for conversion into the lower reservoir of a pumped storage power plant. This leverages the elevation difference between the upper and lower reservoirs to establish a green energy storage system. The current state of the abandoned pit, obtained through Unmanned Aerial Vehicle (UAV) oblique photography, is shown in Figure 3. At present, the abandoned mine pit needs to be excavated along its perimeter to reach the designed excavation depth in the reservoir area. In the project, bench excavation is adopted. However, the construction company needs to analyze the slope safety during excavation and support and reinforce the potential slip risks in time to ensure the safety during construction. Therefore, it is necessary to carry out the slope safety analysis under pre-excavation conditions and post-excavation conditions. The reservoir is assumed to be dry, reservoir-induced pore-water pressure and seepage forces are not considered, and the mechanical parameters corresponding to non-impounded conditions are adopted. Therefore, the calculated safety factors characterize excavation-stage stability only.

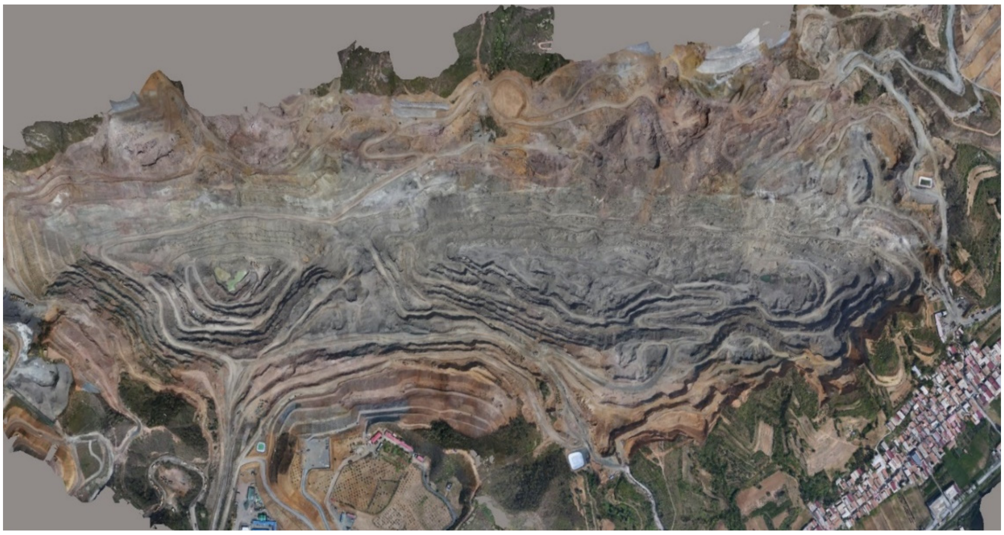

Figure 3. Aerial Photograph of the Abandoned Mine Pit.

The surrounding rock mass for the reservoir roof and floor predominantly consists of pyroxene-amphibolite and hornblende-plagioclase gneiss. These are crystalline massive rocks, and the entire engineering geological rock group is classified as a homogeneous massive rock type. The lithologies of the pyroxene-amphibolite and hornblende-plagioclase gneiss are relatively uniform. The rock mass is dominated by discontinuity planes of Class IV and V with a spacing typically exceeding 100 cm. The rock mass presents as a massive block structure, featuring high-angle shear fissures. Most of these fissure surfaces are closed, and some are infilled with vein rock. The Unconfined Compressive Strength (UCS) of slightly weathered rock and fresh rock ranges from 30 MPa to 60 MPa, whereas the UCS of moderately weathered rock is typically below 30 MPa. Overall, the rock mass quality is classified as moderate. The upper slope is covered by colluvial deposits composed primarily of gravelly soil. These deposits have a variable thickness ranging from 2 m to 5 m. The physical and mechanical parameters of the strata in the investigation area, determined through geological exploration, are presented in Table 1. It is noted that the mechanical parameters for the Weak Fault and the Strongly Weathered Layer are identical in Table 1. This is because the strongly weathered rock mass in this area is highly fractured and decomposed, exhibiting soil-like mechanical properties similar to the fault gouge and cataclasite within the fault zone. To ensure a conservative estimate of slope stability during the excavation phase, the parameters of the weaker fault zone were adopted for the strongly weathered layer. This conservative approach ensures that the calculated safety factors are not overestimated, thereby providing a robust basis for engineering design. The rock layers were modeled with the Mohr-Coulomb constitutive model for the calculation of the slope safety factors.

Table 1. Rock mechanics parameters.

Rock Stratum		Density *r* (kg/m^3)	Internal Friction Angle, φ (°)	Cohesion, C (kPa)	Elastic Modulus, *E* (Gpa)	Poisson's Ratio
Breccia Tuff	Slightly weathered	2440	55.34	5.17	38.10	0.22
	Weakly weathered	2410	55.46	5.25	29.48	0.24
Plagioclase Amphibolite	Slightly weathered	3030	53.5	4.33	27.90	0.25
	Weakly weathered	2600	54.8	4.85	32.50	0.24
Hornblendite		3240	50.55	3.25	42.70	0.22
Weak Fault		2590	51.9	2.70	15.3	0.19
Strongly Weathered Layer		2590	51.9	2.70	15.3	0.19
Colluvial deposits		2200	21.80	7.50	5.0	0.34

3.2. Fault Strike

The F1 fault is a Class II structural plane, located on the northwest bank slope of the lower reservoir, as shown in Figure 4. The fault's hanging wall is defined by the Baiqi Formation (J3b) Tuff Series, while the footwall consists of Late Paleozoic (ψO4) Amphibolite. With a strike length exceeding 3 km, this feature is classified as a Class II structural plane. Within the pit area, the fault exhibits a dominant overall attitude of N65–85° E, NW∠50–80°. A distinct geometric complexity arises along the northwest slope of the West Pit, characterized by severe contortion of the fault plane. The apparent dip direction of the fault reverses locally, transitioning from an anti-dip configuration (dipping into the rock mass) to a dip configuration (daylighting out of the slope face). Farther west on this same slope, it warps once more, returning to a dip towards the slope interior. The specific attitude for the section that dips towards the exterior is recorded as N50–60° E, SE∠60–80°. The fault zone's width is also notably variable, typically measuring 15 m to 30 m, but locally increasing to over 40 m. The fault core demonstrates significant internal heterogeneity in its lithological and structural properties. Characteristically, the upper and lower boundaries are delineated by material composed of cataclasite, foliated rock, and ultracataclasite. These boundary materials generally exhibit poor geotechnical properties due to their loose and incoherent structure. Conversely, the central part of the core is primarily defined by the presence of lenticular bodies. Specifically, the cataclasite zones along the upper and lower interfaces typically measure 3 m to 5 m wide. In localized areas, this material is further observed to consist of mud-matrix supported detritus. Along the northeast side of the lower reservoir, the fault exhibits an attitude of N85° E, NW∠85°. In this area, the fault core scale diminishes, maintaining a width of 3 m to 5 m. The internal structure here is defined by 0.2 m to 0.3 m thick zones of foliated rock that flank a central zone of angular rock fragments (or crushed rock blocks). Further along the strike, specifically on the eastern side of the Habaqin Gully, the fault's attitude changes dramatically to N60° W, SW∠65°. Correspondingly, the width narrows significantly to between 1.5 m and 2.0 m. At this location, the core's lithology is simplified, being composed primarily of foliated rock and cataclasite.

3.3. Typical Geological Analysis Sections

To accurately conduct the safety analysis of the high and steep slopes of the pumped storage power station's lower reservoir area, both before and after excavation, multiple typical geological analysis sections were selected based on the characteristics of the site. The Janbu method and the M-P method were then used to calculate the slope safety factors. Figure 5 illustrates the typical geological analysis sections before excavation, with one calculation analysis section arranged along the reservoir axis and eight analysis sections arranged perpendicular to the reservoir axis. Figure 6 illustrates the typical geological analysis sections after excavation, with five analysis sections arranged along the reservoir axis and five analysis sections arranged perpendicular to the reservoir axis.

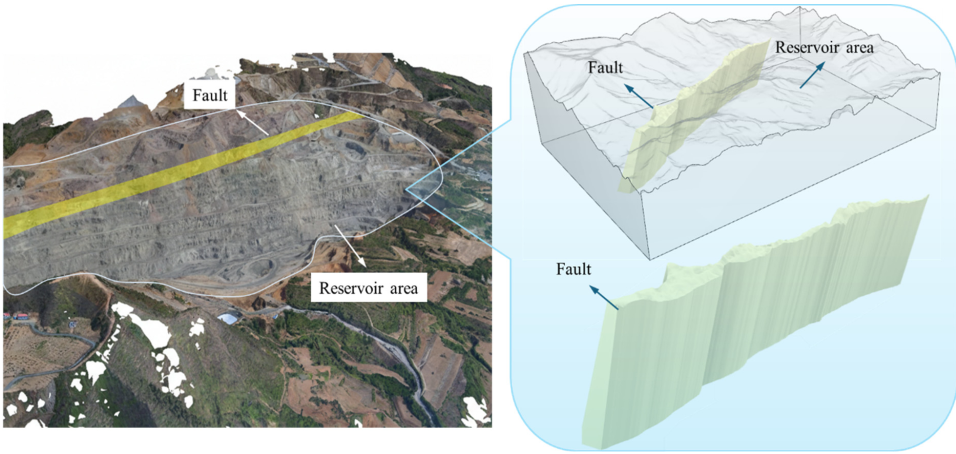

Figure 4. Schematic diagram of the reservoir area with fault.

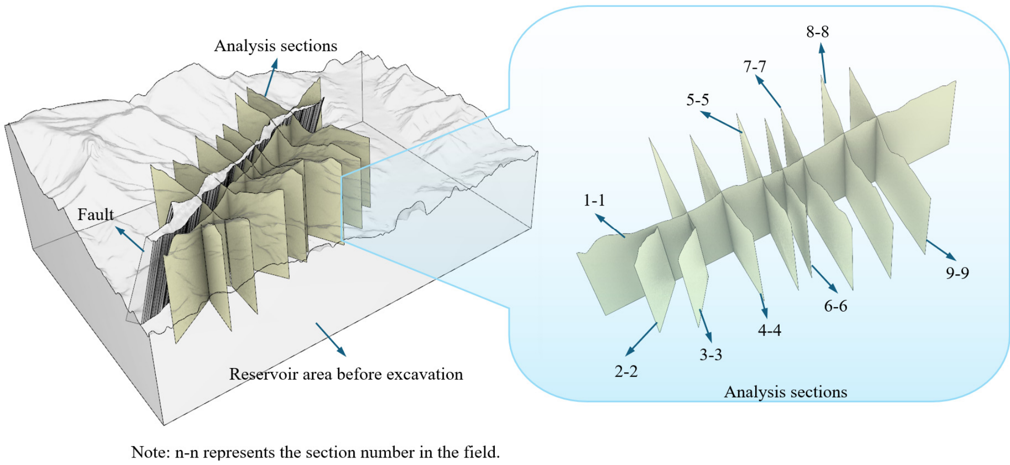

Figure 5. Typical geological analysis sections of the reservoir area under pre-excavation condition.

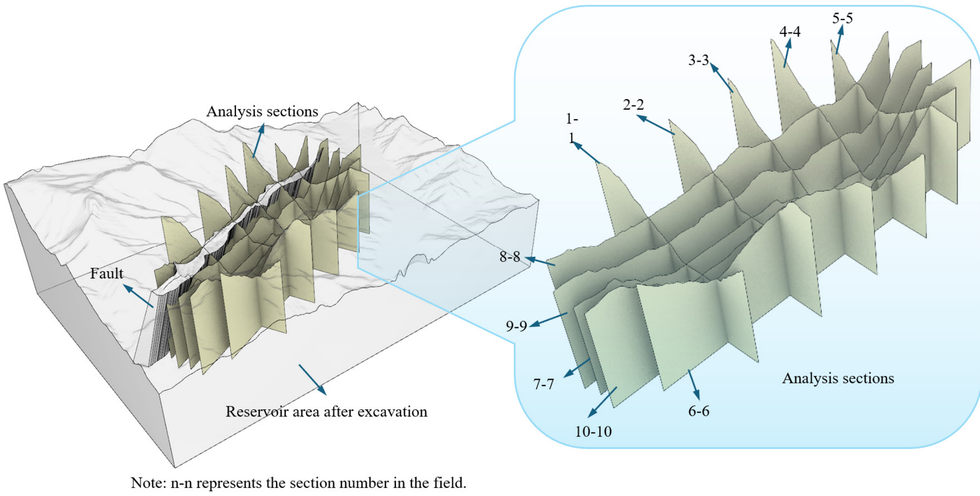

Figure 6. Typical geological analysis sections of the reservoir area under post-excavation condition.

4. Slope Stability Analysis

4.1. Pre-Excavation Condition

Safety analysis of the typical geological analysis sections before excavation was conducted using both the Janbu method and the M-P method, respectively. Appendix A displayed calculation results of some geological sections. In the current figures, the white slip surface represents the critical slip surface identified by the software. The other colored lines represent the trial surfaces generated during the search process. As shown in Figures 7 and A1, the limit equilibrium calculation for the open-pit slope of the lower reservoir area using the Janbu method resulted in an overall safety factor ranging from 1.33 to 9.70. Given the relatively gentle inclination of geological Section 2-2 under pre-excavation conditions, the slope exhibits minimal susceptibility to failure, corresponding to a remarkably high safety factor of 9.70. As shown in Figure 7b, since the outcrop surface of the soft fault is located on a ramp, the slip surface differs from other analysis sections, traversing from the top of the soft fault along an arc to the bottom of the staged excavation. In contrast, the slip surfaces of the remaining typical analysis sections traverse from the slope crest along an arc to the slope toe. Furthermore, the slope slip surface in Figure 7c shows failure occurring on the slope far from the fault, while the slip surfaces in the other analysis sections appear on the slopes where the fault is present. This is primarily because the geological conditions on the slope far from the fault in this particular analysis section are relatively weaker, and the slope ratio (steepness) is greater, resulting in a smaller safety factor compared to the opposite side.

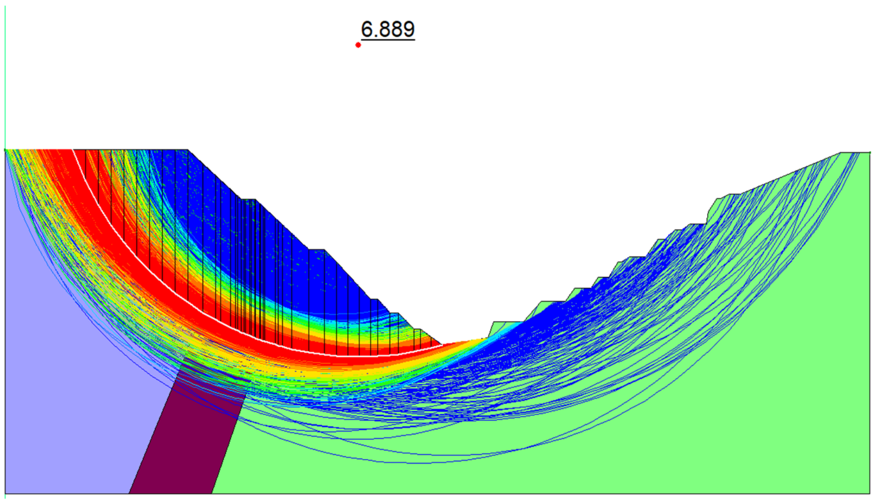

(**a**)

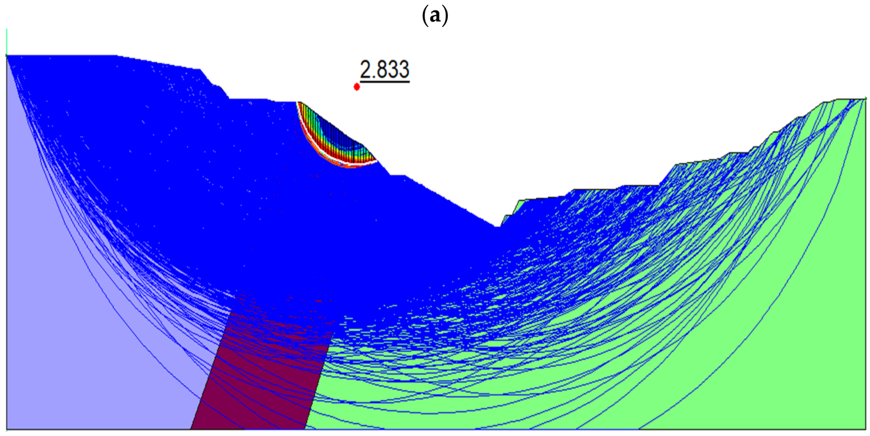

(**b**)

Figure 7. *Cont.*

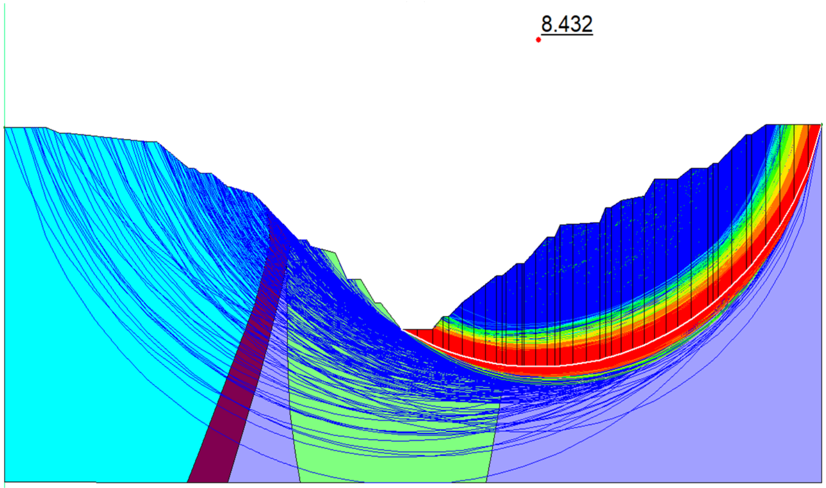

(c)

Figure 7. Janbu Method. (**a**) Section 3-3; (**b**) Section 4-4; (**c**) Section 6-6.

As shown in Figures 8 and A1, the limit equilibrium calculation for the open-pit slope of the lower reservoir area using the M-P method resulted in an overall safety factor ranging from 1.40 to 10.20. While the slope at geological Section 2-2 in the pre-excavation condition is relatively gentle, it is not easy to slip with the safety factor of reaching 10.20. Except for analysis Section 3-3, the trend of the slope slip surface calculated by the M-P method is consistent with the Janbu method. Due to the influence of interslice forces being considered, the safety factor calculated by the M-P method is 5–10% higher than that calculated by the Janbu method. Since the outcrop surface of the soft fault is located on a ramp, the slip surface for analysis Section 3-3 calculated under the M-P method is different from the Janbu method, traversing from the top of the soft fault along an arc to the bottom of the staged excavation; thus, its safety factor is lower than the Janbu method.

4.2. Post-Excavation Condition

The reservoir area slope, with a post-excavation maximum height of 400 m, is classified as a high and steep slope. A stability analysis for the typical geological profile was subsequently performed using two distinct limit equilibrium approaches: the Janbu method and the M-P method. Specifically, as shown in Figures 9 and A3 in Appendix A, the limit equilibrium calculation for the open-pit slope of the lower reservoir area using the Janbu method indicates an overall safety factor ranging from 2.13 to 6.89. As shown in Figure 9a, since the outcrop surface of the soft fault is located on a ramp and occupies a large proportion, the slip surface differs from other analysis sections, traversing from the top of the soft fault along an arc to the bottom of the staged excavation. In contrast, the slip surfaces of the remaining typical analysis sections traverse from the slope crest along an arc to the slope toe. Furthermore, the slope slip surfaces in Figure 9b,c show failure occurring on the slope far from the fault, while the slip surfaces in the other analysis sections appear on the slopes where the fault is present. This is primarily because the slope ratio in these analysis sections is greater, resulting in a smaller safety factor compared to the opposite side.

As shown in Figures 10 and A4, the limit equilibrium calculation for the open-pit slope of the lower reservoir area after excavation using the M-P method resulted in an overall safety factor ranging from 2.47 to 7.04. The trend of the slope slip surface calculated by the M-P method is consistent with that of the Janbu method. Since the influence of interslice forces is considered, the safety factor calculated by the M-P method is generally higher than that calculated by the Janbu method.

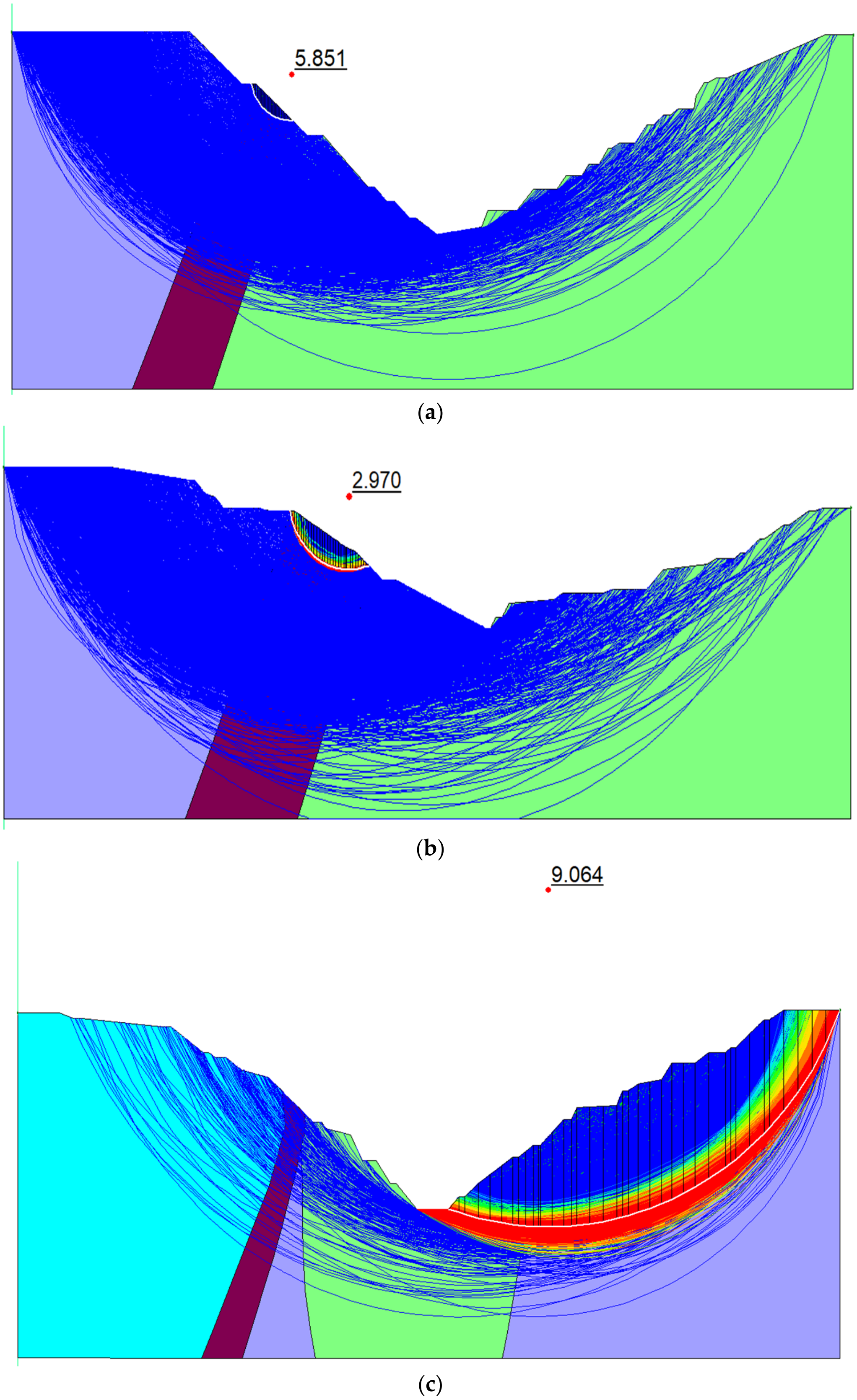

Figure 8. M-P Method. (**a**) Section 3-3; (**b**) Section 4-4; (**c**) Section 6-6.

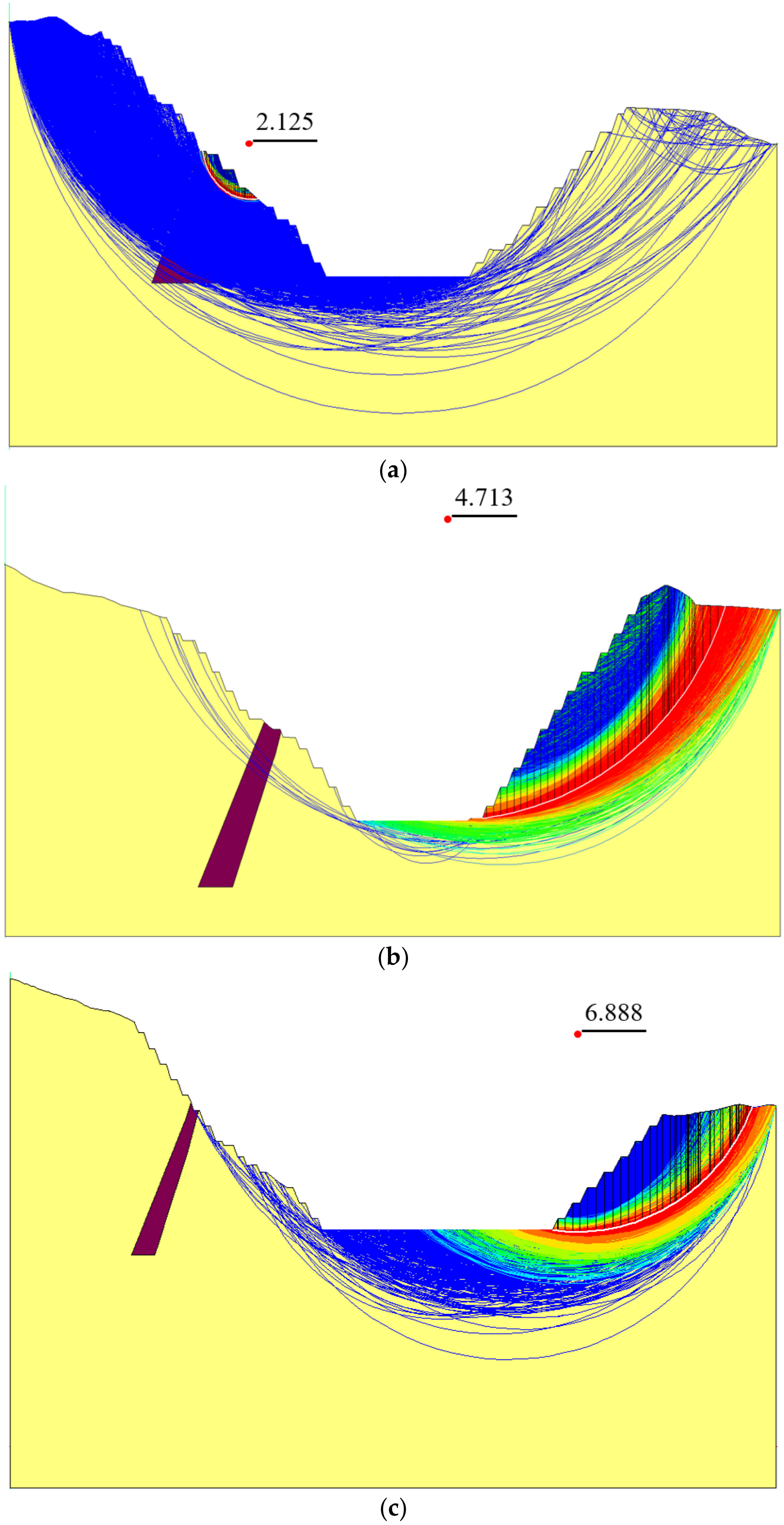

Figure 9. Janbu Method. (**a**) Section 1-1; (**b**) Section 2-2; (**c**) Section 3-3.

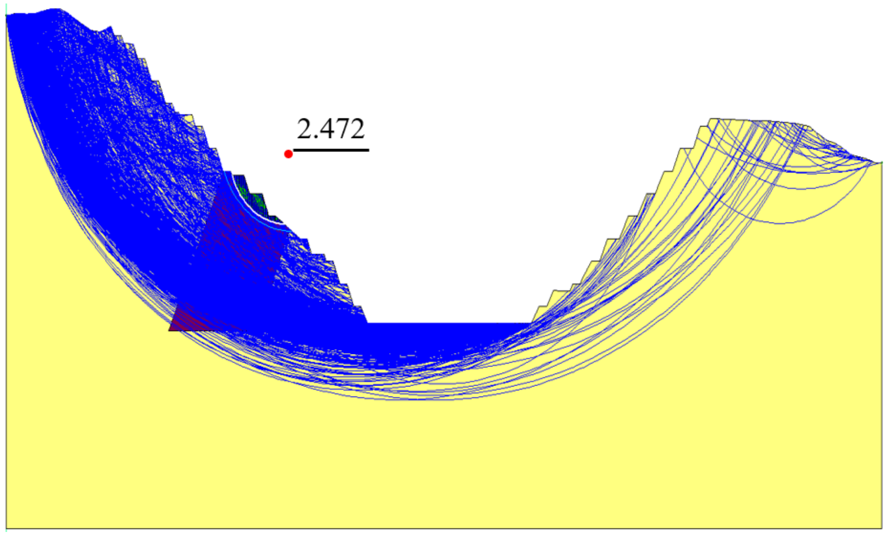

(**a**)

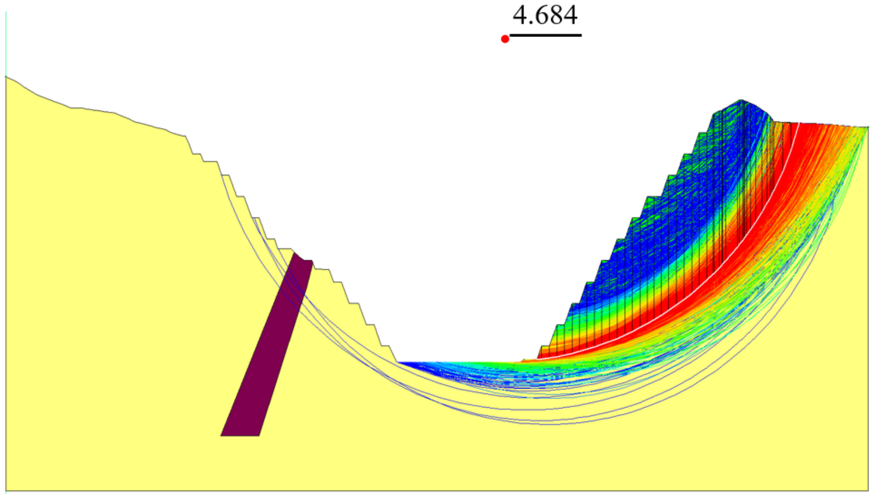

(**b**)

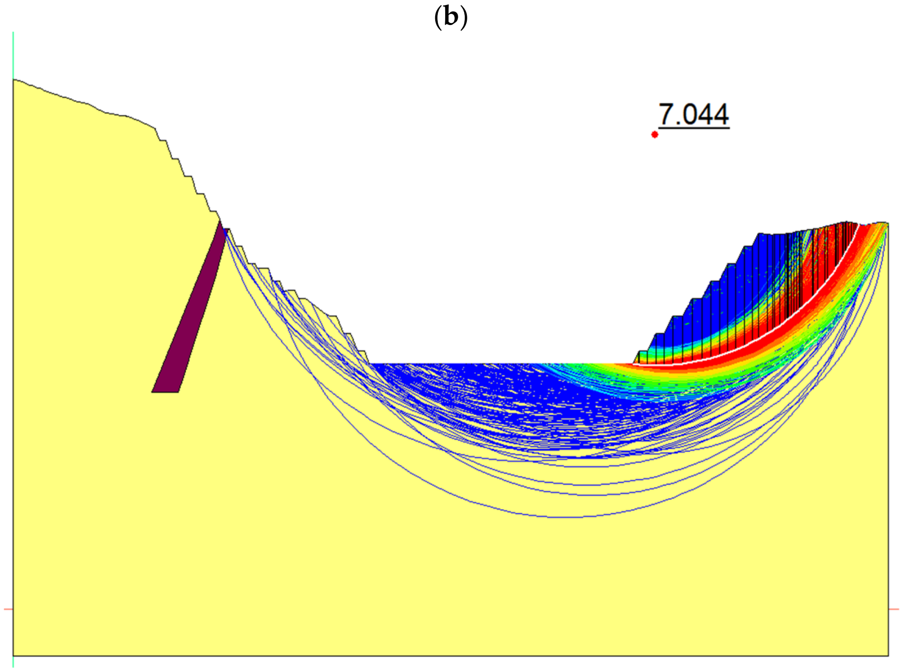

(**c**)

Figure 10. M-P Method. (**a**) Section 1-1; (**b**) Section 2-2; (**c**) Section 3-3.

4.3. Analysis of Stability Results

Figures 11 and 12 statistically summarize the slope safety factors for the typical geological analysis sections of the reservoir area before and after excavation, respectively, and the summary of slope stability analysis results for every analyzed section are listed at Tables A1 and A2 in Appendix A. It is worth noting that the calculation result of Janbu method is lower than that of M-P method. Based on the calculation results of the multiple typical slope geological analysis sections, it can be concluded that the safety factor for the reservoir slope before excavation is greater than the limit value of 1.15 in code (Clause 3.09 in GB 51016-2014) [28], indicating a safe state. Since the areas with a low safety factor in the existing slope are located in colluvial deposits or fault zones, it is recommended during construction that the colluvial deposits be cleared first and that the fault zones be prioritized for excavation. Although the creation of high and steep slopes post-excavation generally induces a reduction in the global safety margin across various geological sections, the systematic clearance of superficial colluvial deposits and weak rock masses during construction effectively mitigates critical failure risks. Consequently, the minimum safety factor experiences a notable increase from 1.33 to 2.13, demonstrating the rationality and efficacy of the slope excavation design in enhancing local stability at the weakest zones. Although the current safety factors fully satisfy the normative requirements, it is conservatively recommended that the fault-affected areas be locally reinforced using reinforced concrete grid beams during the excavation process to further enhance construction safety. It is worth noting that the recommendation to adopt the Janbu method for conservative engineering design is not only based on its lower safety factor estimates but also on its theoretical suitability for the specific geological conditions of this project. The Simplified Janbu method satisfies force equilibrium and makes simplified assumptions about inter-slice forces, often yielding a lower-bound estimate of the safety factor. In contrast, the M-P method, while satisfying both force and moment equilibrium, tends to provide higher safety factor values. For high and steep slopes with weak faults, where the consequences of failure are severe, a conservative approach is paramount. The Janbu method's lower estimates provide a safer margin for risk assessment.

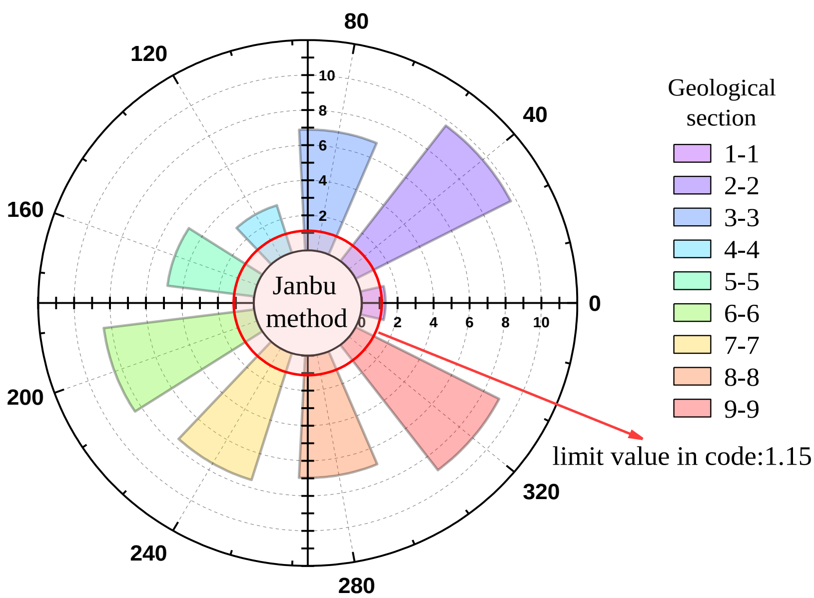

(**a**)

Figure 11. *Cont.*

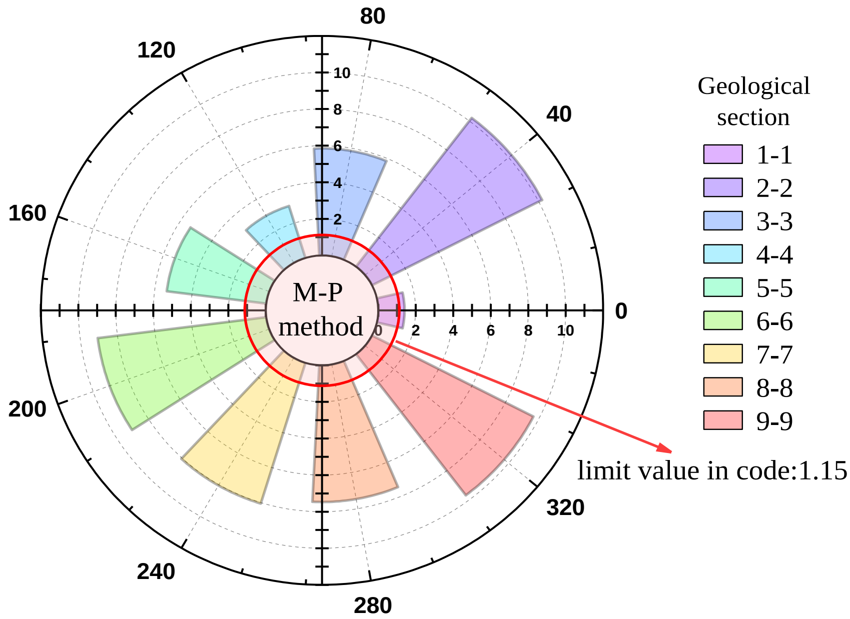

(**b**)

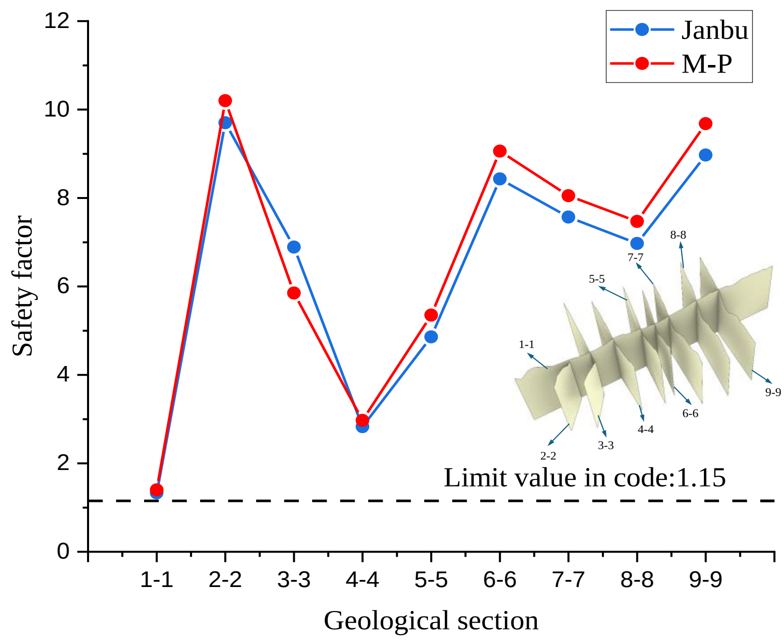

(**c**)

Figure 11. Safety factors for the reservoir slope under pre-excavation condition. (**a**) Janbu method; (**b**) M-P method; (**c**) Result comparison.

4.4. Discussion on Stability Improvement

It is important to clarify the rationale behind comparing the safety factors before (1.33) and after (2.13) excavation. While the overall geometric configurations differ, the comparison is fundamentally based on the stability of the critical geological interface under different stress states. The excavation process serves as a stress unloading measure. By removing the overburden mass and reducing the slope angle, the excavation significantly decreases the driving shear stress acting on the geological model. In pre-excavation condition, the high overburden pressure generates significant shear stress along the fault plane, leading to a lower safety factor. In post-excavation condition, the reduction in overburden weight decreases the shear stress on the fault, while the shear strength governed by material properties remains relatively constant. This leads to a substantial increase in the safety factor.

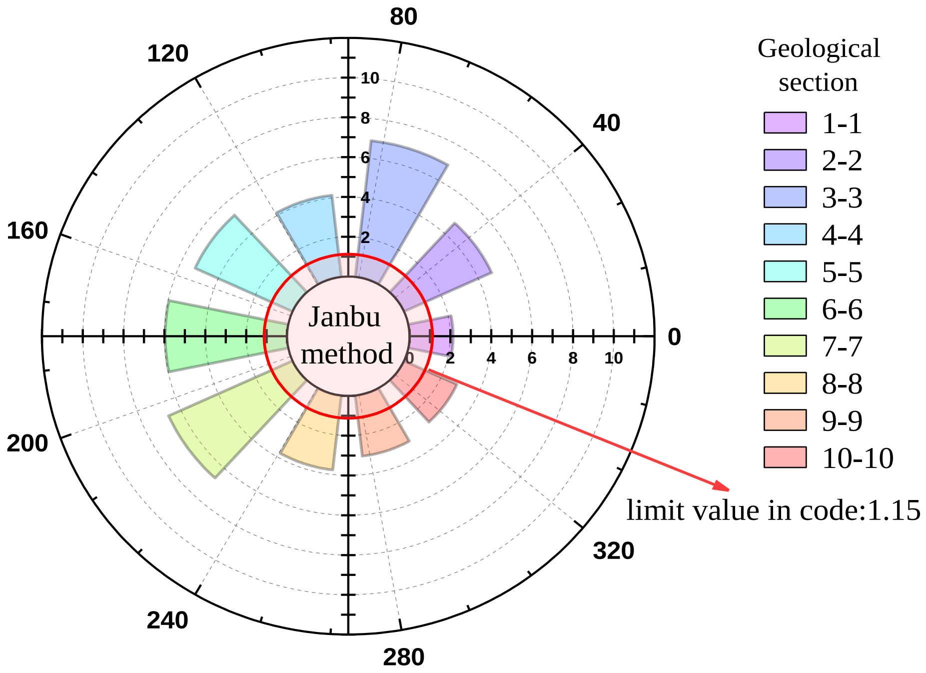

(**a**)

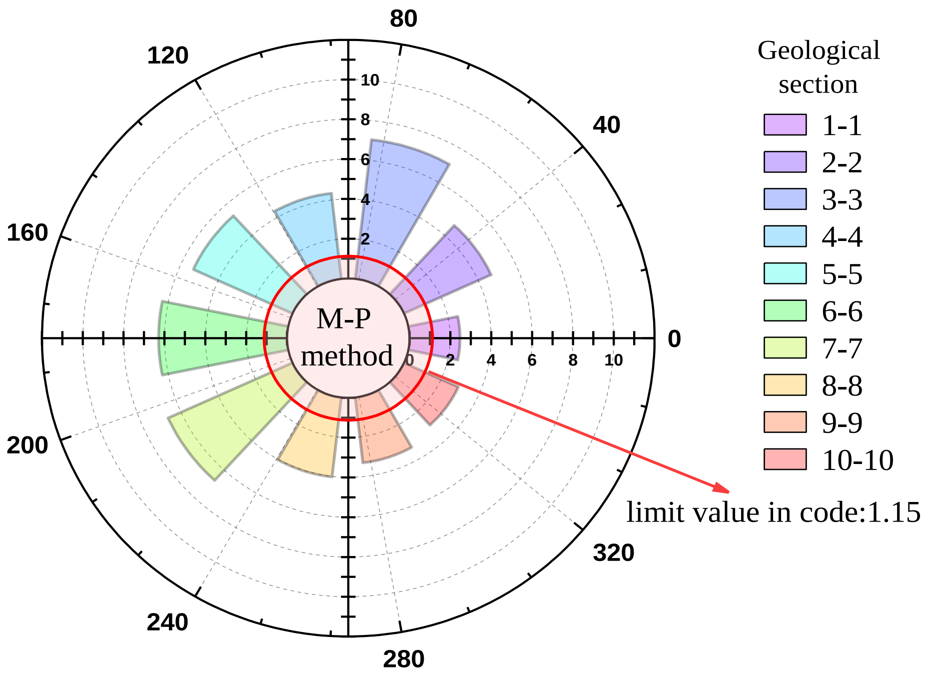

(**b**)

Figure 12. *Cont.*

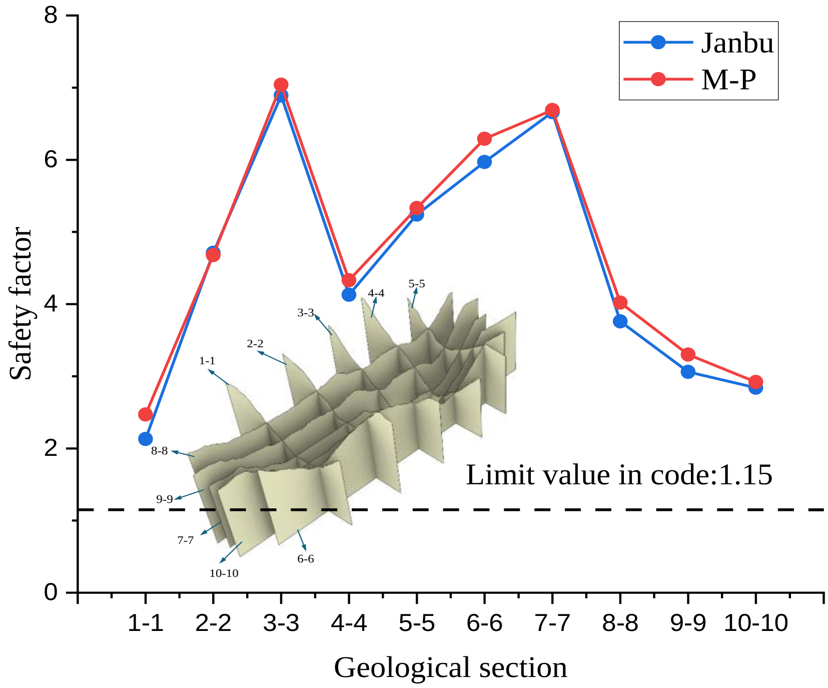

(c)

Figure 12. Safety factors for the reservoir slopes under post-excavation condition. (**a**) Janbu method; (**b**) M-P method; (**c**) Result comparison.

5. Conclusions

This paper addresses the high and steep slope stability issues arising from the conversion of abandoned open-pit mines into pumped storage power station reservoirs. Using the Janbu method and the M-P method, limit equilibrium safety analysis was conducted on typical analysis sections of the reservoir slope both before and after excavation, calculating the slope's failure modes and safety factors. The following conclusions can be drawn:

(1) The calculated safety factor range for the reservoir slope before and after excavation using the M-P method is 1.40–10.20 and 2.47–7.04, respectively. When the position of the slip surface is consistent, the slope safety factor calculated by the M-P method is higher than that calculated by the Janbu method. Therefore, it is conservatively suggested to adopt the Janbu method for slope analysis.

(2) When the outcrop surface of a fault is located on a ramp and occupies a large proportion, the calculated slip surface will traverse from the top of the soft fault along an arc to the bottom of the staged excavation, indicating that the position of the fault has a certain influence on the slope failure mode and the safety factor.

(3) Although the factors of safety for the reservoir slope both before and after excavation are higher than the normative limit value for this project involving a 400 m high slope to ensure construction safety, it is recommended that the colluvial deposits and fault zones—which exhibit lower factors of safety—be cleared first during the excavation stage. Furthermore, to balance structural efficacy with construction feasibility and cost-effectiveness, it is recommended that the fault zones be reinforced using reinforced concrete grid beams after excavation but prior to reservoir impoundment.

It is important to note that the current stability analysis is based on peak strength parameters, which are valid for short-term construction-stage assessments. In contrast, long-term stability is influenced by the degradation of fault gouge strength to residual values. Future research should therefore focus on characterizing these residual parameters to support long-term slope performance evaluation and risk management. Regarding modeling methodology, while the current 2D analysis provides a conservative estimate, future work will adopt 3D numerical modeling (e.g., 3D FEM or DEM) to accurately simulate the 3D kinematic constraints and stress redistribution associated with the irregular pit geometry. Finally, because the current analysis focuses on the construction stage, it does not reflect the destabilizing effects of hydrostatic pressure from future reservoir impoundment. Long-term stability assessments must therefore integrate these critical hydrological factors.

Author Contributions: Conceptualization, H.J. and Q.M.; methodology, H.J. and M.Z.; software, H.J. and J.Z.; validation, H.J., M.Z. and S.H.; formal analysis, H.J. and J.Z.; investigation, H.J. and C.X.; resources, Q.M. and C.X.; data curation, H.J. and J.Z.; writing—original draft preparation, H.J.; writing—review and editing, Q.M., M.Z. and C.X.; visualization, H.J. and S.H.; supervision, Q.M.; project administration, H.J. funding acquisition, H.J., M.Z., C.X. and Q.M. All authors have read and agreed to the published version of the manuscript.

Funding: This research was funded by the National Natural Science Foundation of China (No. 52509174), the Deep Earth Probe and Mineral Resources Exploration-National Science and Technology Major Project (No. 2024ZD1000408), the S&T Program of Chengde (No. 202304B069), and the Open Fund of the State Key Laboratory of Hydraulic Engineering Intelligent Construction and Operation, Tianjin University (No. HESS-2510).

Institutional Review Board Statement: Not applicable.

Informed Consent Statement: Not applicable.

Data Availability Statement: The data that support the findings of this study are available from He Bei Hua Kan Resource Environmental Survey Co., Ltd., but restrictions apply to the availability of these data, which were used under license for the current study, and so are not publicly available. Data are, however, available from the authors upon reasonable request and with permission of He Bei Hua Kan Resource Environmental Survey Co., Ltd.

Acknowledgments: This research was funded by the National Natural Science Foundation of China (No. 52509174), the Deep Earth Probe and Mineral Resources Exploration-National Science and Technology Major Project (No. 2024ZD1000408), the S&T Program of Chengde (No. 202304B069), and the Open Fund of the State Key Laboratory of Hydraulic Engineering Intelligent Construction and Operation, Tianjin University (No. HESS-2510). The authors wish to thank Jialin Wu for providing helpful discussions and assisting with data collection.

Conflicts of Interest: Author Huihui Jia was employed by the company He Bei Hua Kan Resource Environmental Survey Co., Ltd. The remaining authors declare that the research was conducted in the absence of any commercial or financial relationships that could be construed as a potential conflict of interest.

Appendix A

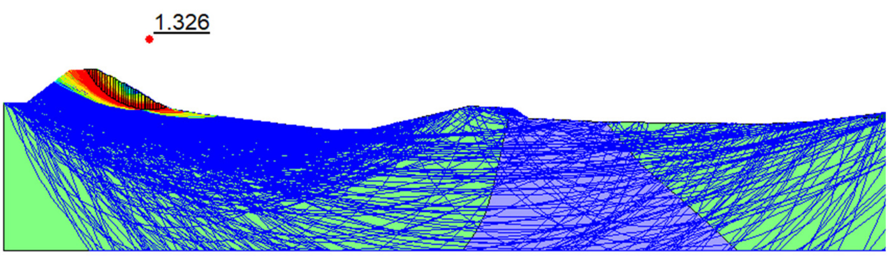

(**a**)

Figure A1. *Cont.*

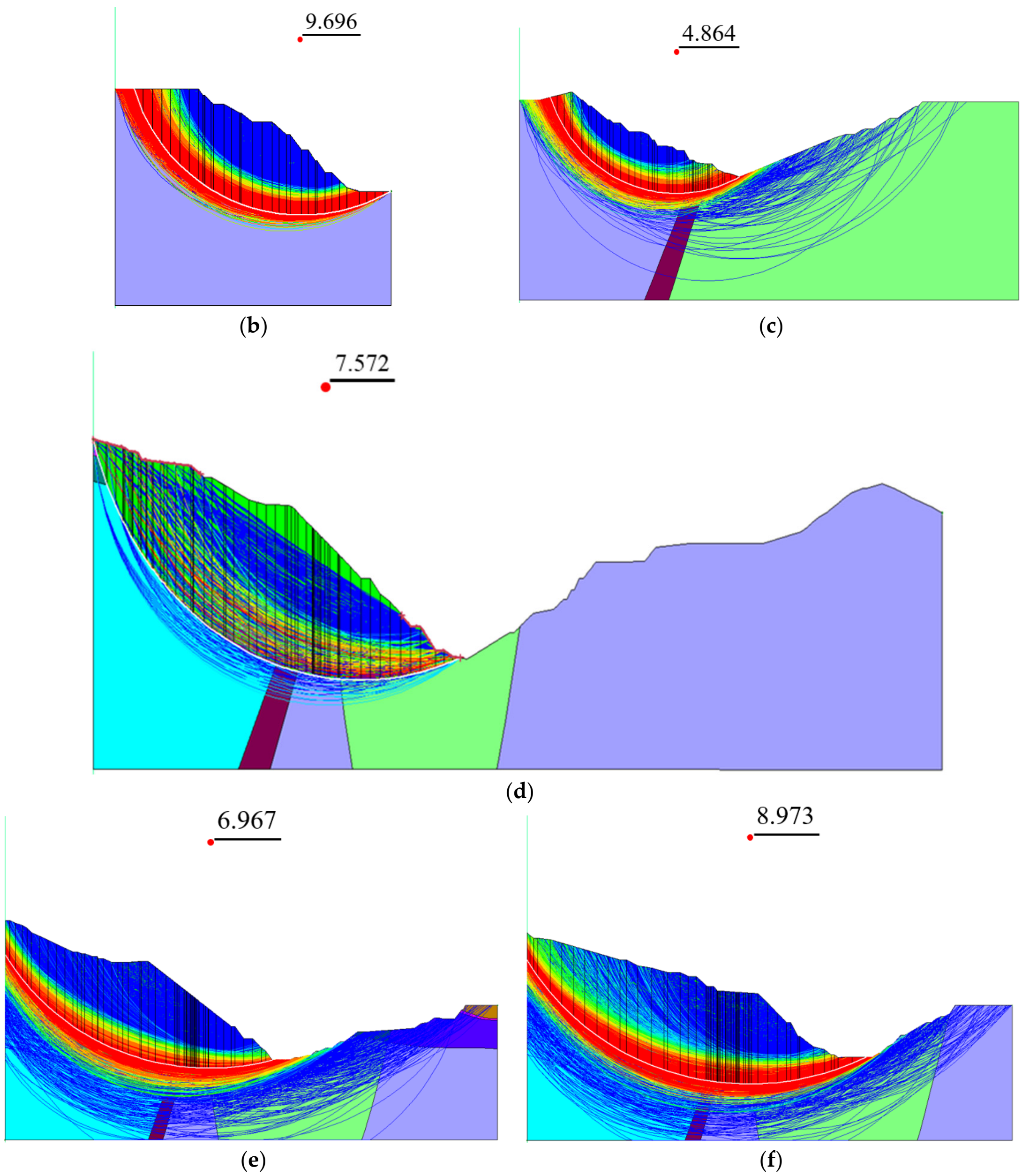

Figure A1. Janbu Method. (**a**) Section 1-1; (**b**) Section 2-2; (**c**) Section 5-5; (**d**) Section 7-7; (**e**) Section 8-8; (**f**) Section 9-9.

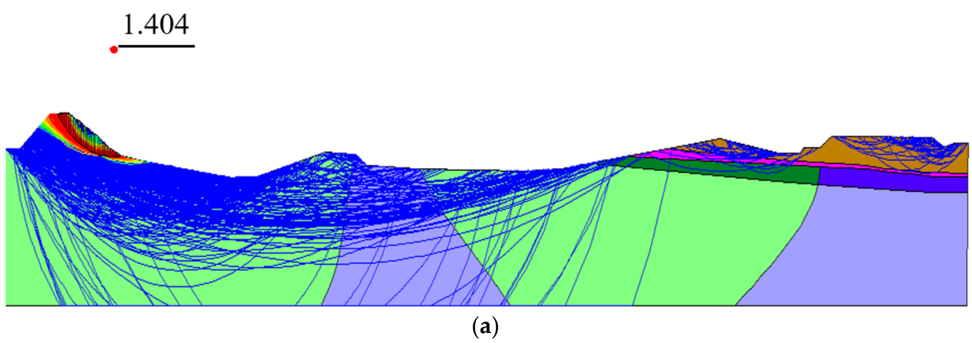

Figure A2. *Cont.*

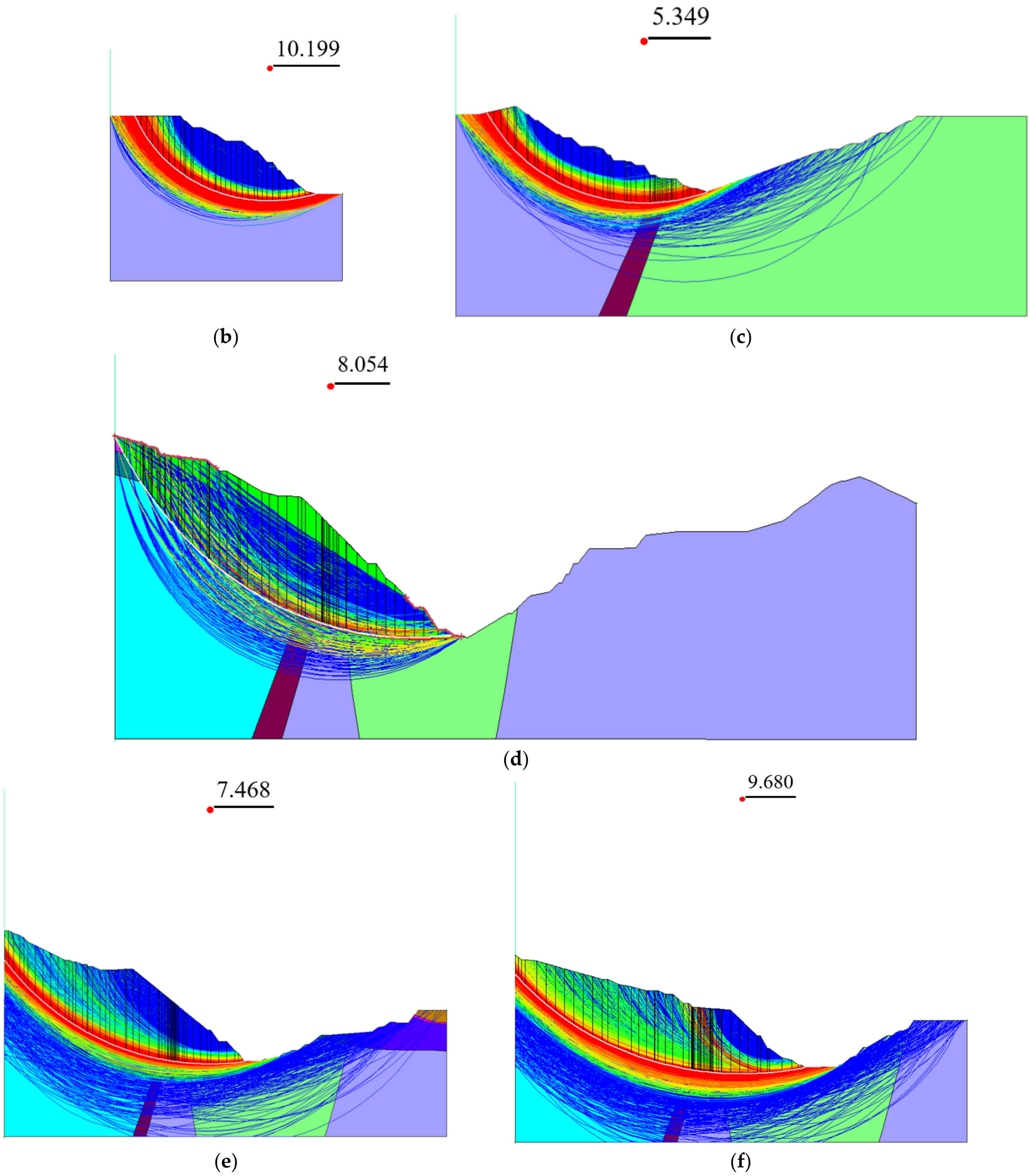

Figure A2. M-P Method. (**a**) Section 1-1; (**b**) Section 2-2; (**c**) Section 5-5; (**d**) Section 7-7; (**e**) Section 8-8; (**f**) Section 9-9.

Table A1. Summary of slope stability analysis results under pre-excavation condition.

Section	Fs (Janbu)	Fs (M-P)	Slope Height (m)	Failure Mode Classification
1-1	1.33	1.4	112.2	Crest-to-toe
2-2	9.7	10.2	133.3	Crest-to-toe
3-3	6.89	5.85	176.0	Fault-controlled
4-4	2.83	2.97	139.0	Fault-controlled
5-5	4.86	5.35	149.0	Crest-to-toe
6-6	8.43	9.06	182.1	Crest-to-toe
7-7	7.57	8.05	224.0	Crest-to-toe
8-8	6.97	7.47	280.0	Crest-to-toe
9-9	8.97	9.68	235.3	Crest-to-toe

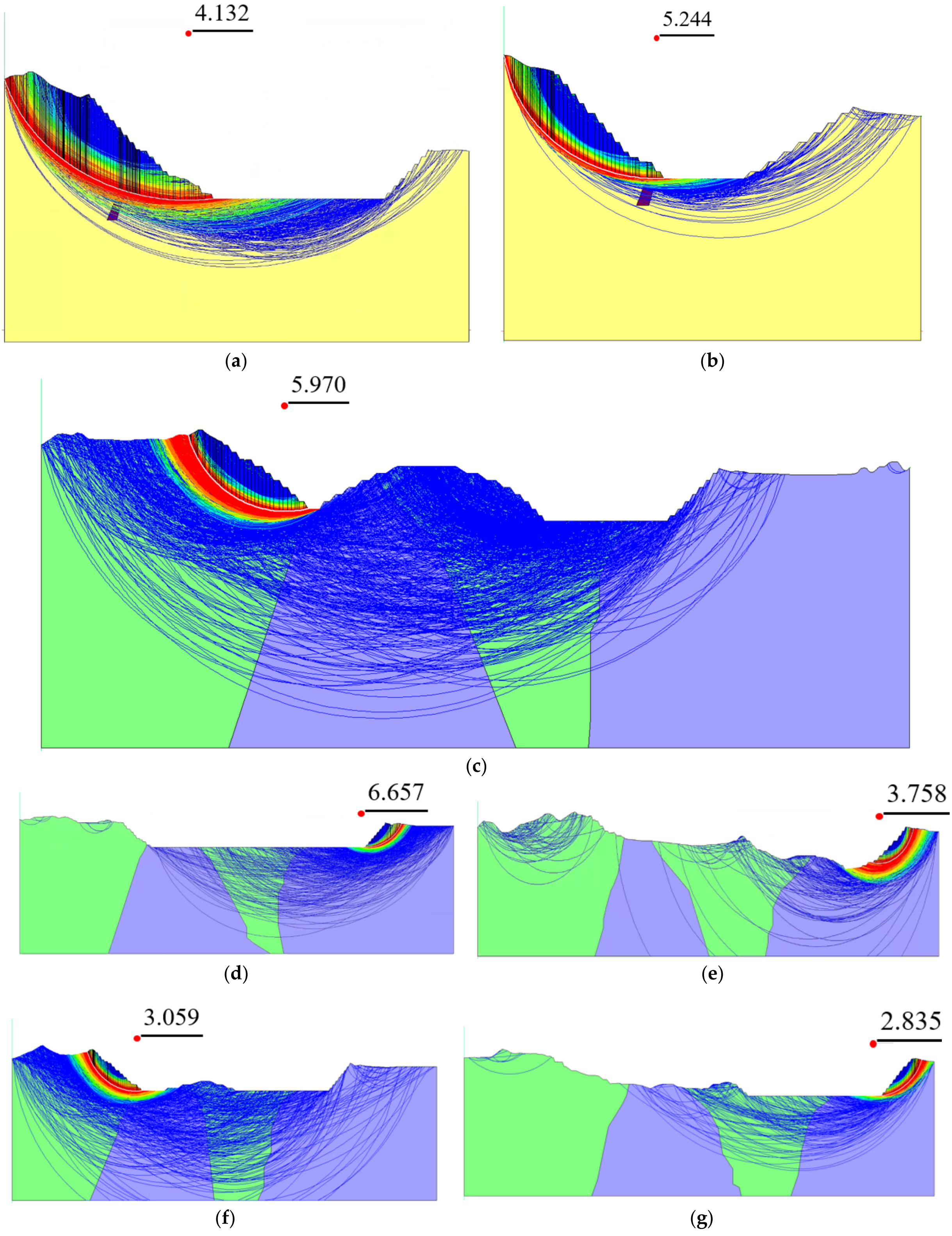

Figure A3. Janbu Method. (**a**) Section 4-4; (**b**) Section 5-5; (**c**) Section 6-6; (**d**) Section 7-7; (**e**) Section 8-8; (**f**) Section 9-9; (**g**) Section 10-10.

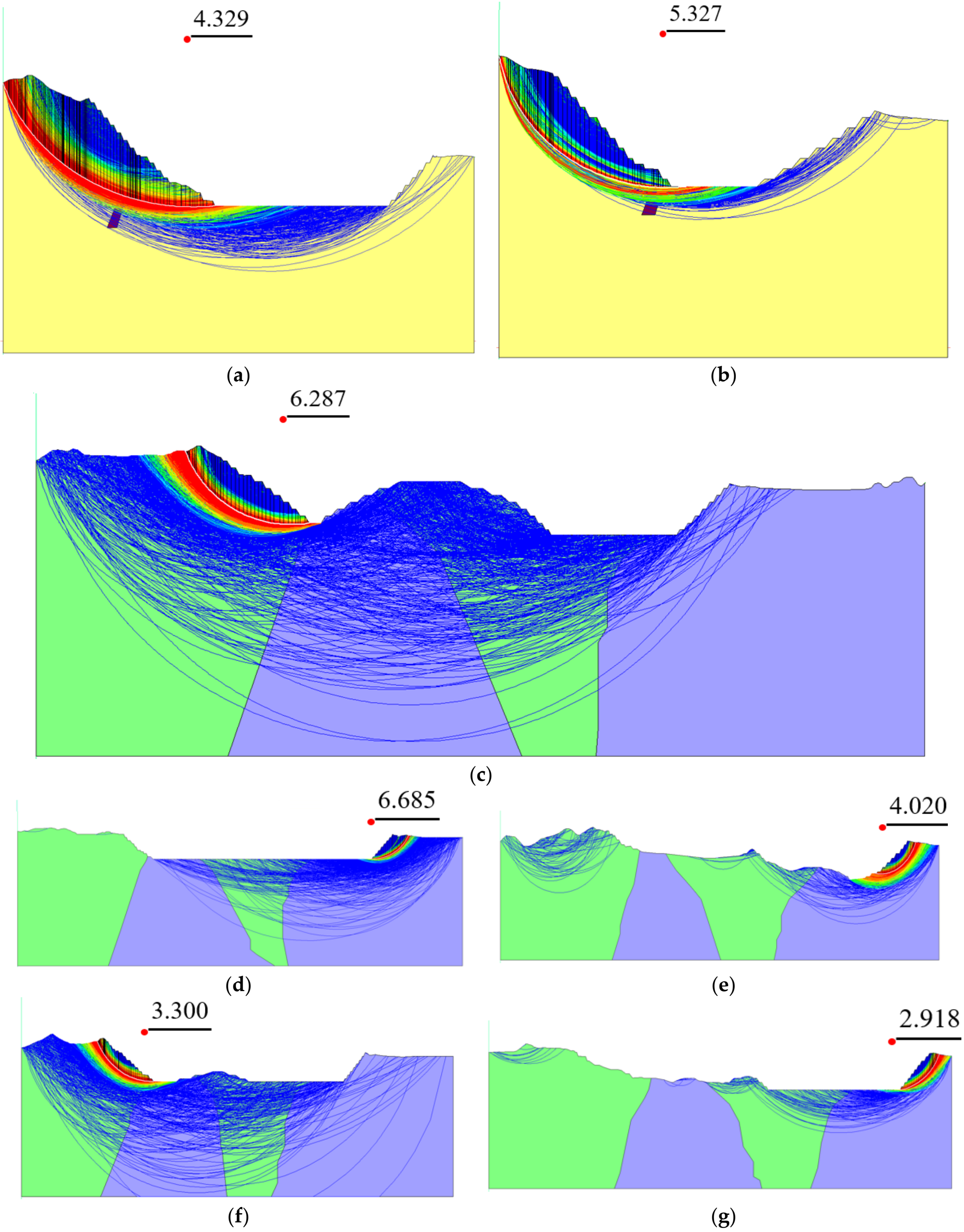

Figure A4. M-P Method. (**a**) Section 4-4; (**b**) Section 5-5; (**c**) Section 6-6; (**d**) Section 7-7; (**e**) Section 8-8; (**f**) Section 9-9; (**g**) Section 10-10.

Table A2. Summary of slope stability analysis results under post-excavation condition.

Section	Fs (Janbu)	Fs (M-P)	Slope Height (m)	Failure Mode Classification
1-1	2.13	2.47	334.0	Fault-controlled
2-2	4.71	4.68	320.2	Crest-to-toe
3-3	6.89	7.04	391.0	Crest-to-toe
4-4	4.13	4.33	417.0	Crest-to-toe
5-5	5.24	5.33	306.1	Crest-to-toe
6-6	5.97	6.29	267.0	Crest-to-toe
7-7	6.66	6.69	186.0	Crest-to-toe
8-8	3.76	4.02	204.9	Crest-to-toe
9-9	3.06	3.3	277.7	Crest-to-toe
10-10	2.84	2.92	206.3	Crest-to-toe

References

1. Menéndez, J.; Schmidt, F.; Konietzky, H.; Fernández-Oro, J.M.; Galdo, M.; Loredo, J.; Díaz-Aguado, M.B. Stability analysis of the underground infrastructure for pumped storage hydropower plants in closed coal mines. *Tunn. Undergr. Space Technol.* **2019**, *94*, 103117. [CrossRef]
2. Yang, K.; Fu, Q.; Yuan, L.; Liu, Q.; He, X.; Liu, F. Research on development demand and potential of pumped storage power plants combined with abandoned mines in China. *J. Energy Storage* **2023**, *63*, 106977. [CrossRef]
3. Song, Z.; Zhao, Y.; Blöcher, G.; Tian, D.; Petrova, E.; Wang, F.; Khaledi, K. Coal mine underground water reservoirs: A sustainable water storage solution for mining areas. *Tunn. Undergr. Space Technol.* **2026**, *168*, 107143. [CrossRef]
4. Sun, Z.; Zhao, Y.; Bolz, P.; Côte, C.; Ren, J. A multimethod GIS-based framework for site selection of underground pumped storage power stations using closing coal mines: A case study of the Shanxi province, China. *Renew. Energy* **2025**, *243*, 122521. [CrossRef]
5. Li, M.; Chen, C.; Liang, H.; Han, S.; Ren, Q.; Li, H. Refined implicit characterization of engineering geology with uncertainties: A divide-and-conquer tactic-based approach. *Bull. Eng. Geol. Environ.* **2024**, *83*, 282. [CrossRef]
6. Zhang, J.; Han, S.; Li, M.; Li, H.; Zhao, W.; Wang, J.; Liang, H. CasMDN: A deep learning-based multivariate distribution modelling approach and its application in geotechnical engineering. *Comput. Geotech.* **2024**, *168*, 106164. [CrossRef]
7. Han, S.; Li, M.; Wang, G. Copula-based simulating and analyzing methods of rock mass fractures. *Comput. Geotech.* **2020**, *127*, 103779. [CrossRef]
8. Qiao, P.; Lan, S.; Gu, H.; Mao, Z. Simulation of Underground Reservoir Stability of Pumped Storage Power Station Based on Fluid-Structure Coupling. *CMES-Comp. Model. Eng. Sci.* **2024**, *139*, 1381–1399. [CrossRef]
9. Kafle, L.; Xu, W.-J.; Zeng, S.-Y.; Nagel, T. A numerical investigation of slope stability influenced by the combined effects of reservoir water level fluctuations and precipitation: A case study of the Bianjiazhai landslide in China. *Eng. Geol.* **2022**, *297*, 106508. [CrossRef]
10. Hu, Y.; Lu, Y.; Zheng, Y. Numerical study on seepage-induced instability of soil-rock mixture slopes using CFD-DEM coupling method. *Comput. Geotech.* **2025**, *183*, 107206. [CrossRef]
11. Zhang, J.; Li, M.; Han, S. Seismic Analysis of Gravity Dam–Layered Foundation System Subjected to Earthquakes with Arbitrary Incident Angles. *Int. J. Geomech.* **2022**, *22*, 04021279. [CrossRef]
12. Wang, L.; Lei, Q. Modelling the pre- and post-failure behaviour of faulted rock slopes based on the particle finite element method with a damage mechanics model. *Comput. Geotech.* **2023**, *153*, 105057. [CrossRef]
13. Zeng, Q.; Liao, J.; Ke, H.; Wang, S.; Liu, W.; Chen, B.; Liu, Z.; Zhou, C. Correlation between deep and surface deformations of excavated slopes on the margins of strike-slip fault-depression basins under rainfall conditions. *Eng. Geol.* **2025**, *355*, 108219. [CrossRef]
14. Beynon, S.J.; Faulkner, D.R. Dry, damp, or drenched? The effect of water saturation on the frictional properties of clay fault gouges. *J. Struct. Geol.* **2020**, *140*, 104094. [CrossRef]
15. Gong, F.; Song, Y.; Zeng, L.; Peng, S.; Zou, G.; Wang, G. Effect of fluid saturation on the elastic properties of carbonate rocks with different pore structures in a strike-slip fault zone. *Geoenergy Sci. Eng.* **2025**, *255*, 214110. [CrossRef]
16. Dyson, A.P.; Griffiths, D.V. An efficient strength reduction method for finite element slope stability analysis. *Comput. Geotech.* **2024**, *174*, 106593. [CrossRef]
17. Hua, C.; Yao, L.; Song, C.; Ni, Q.; Chen, D. A New Criterion for Defining Inhomogeneous Slope Failure Using the Strength Reduction Method. *CMES-Comp. Model. Eng. Sci.* **2022**, *132*, 413–434. [CrossRef]
18. Yang, Y.; Xia, Y.; Zheng, H.; Liu, Z. Investigation of rock slope stability using a 3D nonlinear strength-reduction numerical manifold method. *Eng. Geol.* **2021**, *292*, 106285. [CrossRef]
19. Wei, Y.; Jiaxin, L.; Zonghong, L.; Wei, W.; Xiaoyun, S. A strength reduction method based on the Generalized Hoek-Brown (GHB) criterion for rock slope stability analysis. *Comput. Geotech.* **2020**, *117*, 103240. [CrossRef]
20. Brilli, N.; Masi, E.B.; Rossi, G.; Tofani, V. Slope stability modelling of shallow landslides at a regional scale: Comparing two physically-based distributed models. *Geoenviron. Disasters* **2025**, *12*, 18.
21. Shi, C.; Qiao, T.; Xue, D.; Wu, S.; Zhang, C. Dynamic responses and stability analysis of a large-scale slope deposit under non-uniform seismic input. *Geoenviron. Disasters* **2025**, *12*, 19. [CrossRef]
22. Zhou, X.P.; Cheng, H. The long-term stability analysis of 3D creeping slopes using the displacement-based rigorous limit equilibrium method. *Eng. Geol.* **2015**, *195*, 292–300. [CrossRef]
23. Schlotfeldt, P.; Elmo, D.; Panton, B. Overhanging rock slope by design: An integrated approach using rock mass strength characterisation, large-scale numerical modelling and limit equilibrium methods. *J. Rock Mech. Geotech. Eng.* **2018**, *10*, 72–90. [CrossRef]
24. Liu, X.; Li, D.-Q.; Cao, Z.-J.; Wang, Y. Adaptive Monte Carlo simulation method for system reliability analysis of slope stability based on limit equilibrium methods. *Eng. Geol.* **2020**, *264*, 105384. [CrossRef]

25. Wu, Y.; Li, W.; Wu, Z. Slope reliability analysis of high rockfill dams considering stress-coupled spatial variability of friction angle. *Reliab. Eng. Syst. Safe* **2026**, *265*, 111597. [CrossRef]
26. Xu, Y.-B.; Liu, L.-L. Copula-based conditional reliability analysis of slopes in spatially variable soils. *Reliab. Eng. Syst. Safe* **2026**, *265*, 111522. [CrossRef]
27. Zhang, W.; Ran, B.; Gu, X.; Zhang, Y.; Zou, Y.; Wang, P. Efficient reliability analysis of unsaturated slope stability under rapid drawdown using XGBoost-based surrogate model. *Soils Found.* **2024**, *64*, 101539. [CrossRef]
28. *GB 51016—2014[S]*; Ministry of Housing and Urban-Rural Development of the People's Republic of China. Technical Code for Non-Coal Open–Pit Mine Slope Engineering. China Planning Press: Beijing, China.

https://doi.org/10.3390/app16188953